stress of a cylindrical tube subjected to combined axial and radial pressure is about one-sixth of the axial buckling value of a corresponding cylindrical tube. As the ratio of circumferential compressive stress to axial compressive stress increases, as expected, the critical axial buckling stress value decreases. It is also found that the critical buckling stress for combined axial and radial compressive cases investigated here is independent of n.

The nondimensional critical axial strain values of σ_{cr}/E vs t/R ratios for $\eta = 0$, $\eta = 1$, and $\eta = 2$ are plotted in Fig. 2. The buckling interaction curves for combined circumferential and axial compression for clamped cylinders (i.e., for $\eta = 1$ and $\eta = 2$) appear to follow almost a straight line parallel to theoretical classical values for uniform axial compression (i.e., for $\eta = 0$), indicating a uniform percentage decrease in the axial compressive load. The experimental results of V. I. Weingarten and P. Seide[6] for cylinders with simply supported edge conditions indicated the same phenomena observed in this study for clamped cylinders, that the interaction curve between external pressure and axial compression depends on the ratio of thickness to radius.

References

[1]Fung, Y. C. and Sechler, E. E., "Instability of Thin Elastic Shells," *Structural Mechanics, Proceedings of the First Symposium on Naval Structural Mechanics,* Pergamon Press, 1960.

[2]Flügge, W., *Handbook of Engineering Mechanics,* McGraw-Hill, New York, 1962.

[3]Gerard, G. and Becker, H., "Handbook of Structural Stability Part III, Buckling of Curved Plates and Shells," TN D-163, 1959, NACA.

[4]Gerard, G., "Handbook of Structural Stability Part III, Buckling of Curved Plates and Shells," TN D-163, 1959, NACA.

[5]Donnell, L. H., "Stability of Thin Walled Tubes Under Torsion," Rept. 479, 1933, NACA.

[6]Weingarten, V. I. and Seide, P., "Elastic Stability of Thin Walled Cylindrical and Conical Shells Under Combined External Pressure and Axial Compression," *Journal of American Institute of Aeronautics and Astronautics,* Vol. 3, No. 5, May 1965.

FEBRUARY 1974 J. AIRCRAFT VOL. 11, NO. 2

Advanced Beaded and Tubular Structural Panels

Max D. Musgrove* and Bruce E. Greene†
Boeing Aerospace Company, Seattle, Wash.
and
John L. Shideler‡ and Herman L. Bohon§
NASA-Langley Research Center, Hampton, Va.

A review is presented of an NASA program to develop lightweight beaded and tubular structural panels which can be applied where beaded external surfaces are acceptable acerodynamically or where primary structure is protected by heat shields. The design shapes were obtained with an optimization computer code which interates geometric parameters to satisfy strength, stability and weight constraints. Methods of fabricating these new configurations are discussed. Nondestructive testing produced extensive combined compression, shear and bending test data on local buckling specimens and large panels. The optimized design concepts offer 25 to 40% weight savings compared to conventional stiffened sheet construction.

I. Introduction

FOR several years Langley Research Center and other NASA agencies have been investigating structural concepts which use elements with curved cross sections to develop beaded or corrugated skin panel structure.[1-5] The curved sections exhibit high local buckling strength which leads to highly efficient structural concepts. These concepts can be applied where a lightly beaded external surface is aerodynamically acceptable or where the primary structure is protected by heat shields. Their corrugated nature makes them especially attractive for high temperature application because the controlled thermal growth minimizes thermal stress. The technology resulting from this program is applicable to many areas such as launch vehicles, space shuttle, and hypersonic aircraft.

A contractual study (NAS1-10749) is in progress by The Boeing Company to develop lightweight structural panels designed for combined loads of inplane compression, inplane shear and bending due to lateral pressure. Under this contract, governing analytical static strength equations for panels under combined load, and material and geometric constraint equations were incorporated in a random search type optimization computer program[6] to identify minimum weight designs for several potentially efficient concepts. However, if these concepts are to realize their analytical potential, all failure modes must be properly recognized and accounted for. Consequently, buckling tests were conducted on subpanels to identify local failure modes and provide for proper modification of local buckling theory. Also, full scale panels (40 × 40 in.) were tested under combined loading to obtain large panel failure data for correlation with theory. A nondestructive force-stiffness test technique[7] was used to provide exten-

Presented as Paper 73-370 at the AIAA/ASME/SAE 14th Structures, Structural Dynamics, and Materials Conference, Williamsburg, Virginia, March 20-22, 1973; submitted April 26, 1973; revision received December 18, 1973. The authors wish to express their thanks to G. A. Jensen for preparing the drafts of this paper.

Index categories: Aircraft Structural Design (Including Loads); Structural Design, Optimal; Structural Static Analysis.

*Senior Specialist Engineer, Structural Allowables and Military Structures, Research and Engineering Division. AIAA Member.

†Senior Specialist Engineer, Structural Allowables and Military Structures, Research and Engineering Division.

‡ Aerospace Engineer, Thermal Section, Structures and Dynamics Division.

§ Head, Thermal Structures Section, Structures and Dynamics Division. AIAA Member.

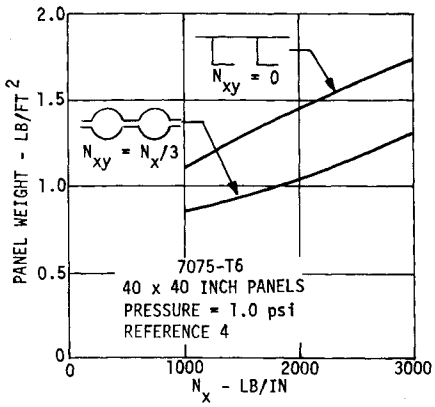

Fig. 1 Compression panel weight vs end load.

sive test results from a comparatively few test panels. This paper presents a summary of the structural panel development program including 40 × 40 in. panel test results and preliminary correlation with theory.

II. Problem Statement

Many recent high performance vehicle designs, particularly the space shuttle orbiter, employ large thick low aspect ratio wings which are lightly loaded. Figure 1, which shows optimum panel unit weight as a function of compressive load,[4] indicates that tubular panels designed for combined axial compression, lateral pressure, and shear are 25 to 40% lighter than conventional stiffened panels designed for corresponding magnitudes of compression and pressure without shear.

Plans to exploit the potential of curved elements in beaded and tubular panels included the following major steps: 1) identify optimum design shapes for single sheet and double sheet panels recognizing manufacturing limits and available analytical data; 2) fabricate and test specimens to determine local failure loads and correlate results with the theory; and 3) fabricate and test panel specimens to define the failure surfaces due to combined loads.

It was necessary to select a structural material, a panel size and specific load combinations for use in comparing the different panel configurations. 7075-T6 aluminum was selected to provide a high proportional limit and ease of fabrication. The high proportional limit is desirable for developmental testing,[8] otherwise test failures occur well into the inelastic range and specimen stability characteristics are obscured by material behavior. 40 × 40 in. panels with the beads terminated at the supports and two specific loading combinations were selected as typical of space shuttle orbiter wing designs. The loading conditions are: 1) 600 lb/in. axial compression, 200 lb/in. inplane shear and 1 psi lateral pressure, and 2) 2000 lb/in. compression, 400 lb/in. shear and 2 psi pressure. Only room temperature is considered.

III. Configuration Optimization

Static strength analysis is the foundation upon which the panel design optimization is based. To obtain a valid optimum panel design, all possible failure modes must be recognized and provided for in the analysis. Three categories of failure modes are considered: 1) general instability; 2) local instability; and 3) material yield. Only failures involving the uniform section, or central region, of the panel are considered here. Panel end closure, joint, and attachment details are assumed adequate to transmit loads necessary to develop full panel strength.

The basic configurations that have been selected for detailed investigation in this program are shown in Fig. 2. The last number in the configuration designation corresponds to the design load condition. The geometry of the fluted single sheet (1a-1) and the fluted tube (2a-1) correspond to optimum designs for load condition 1 and the geometry of configurations (2-2) and (2a-2) correspond to optimum designs for load condition 2.

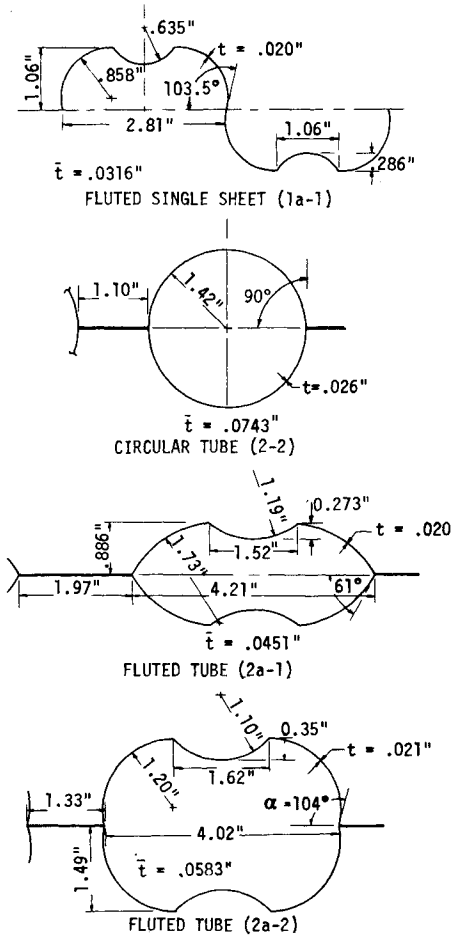

Fig. 2 Optimized developmental configurations.

General Instability

General instability consists of buckling of the entire panel. Available classical solutions for rectangular, simply supported, orthotropic plates are used for elastic failure criteria. However, for highly orthotropic panels of the types considered here, the compression buckling load was taken as the wide-column Euler load. General instability under combined loading in compression and shear is determined by the standard interaction equation,

$$R_c + R_s^2 = 1$$

where R_c and R_s are ratios of applied stress to the critical stress for panel general instability in compression and shear, respectively.

Local Instability

Local instability is defined here as buckling of one or more elements of the panel cross section with buckle half-wave lengths which are small compared to the panel length. Flat elements of the panel cross section are analyzed for local instability in compression and shear as long, simply supported, isotropic plates using available classical solutions.[9] Circular portions of the panel cross section are analyzed for local instability in axial compression and bending using Ref. 10, and in shear using Ref. 11. Local instabilities under combined compression, shear and lateral bending loads are determined by interaction

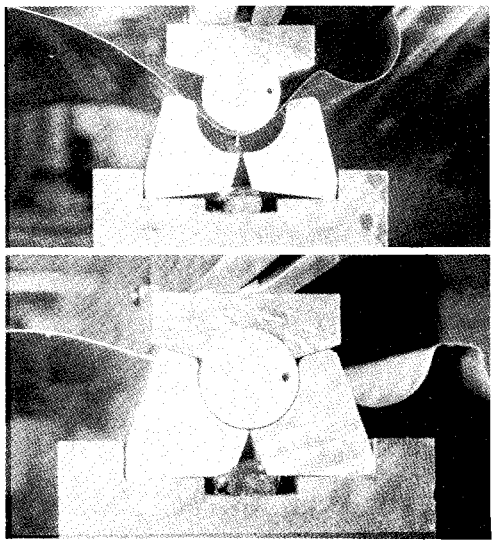

Fig. 3 Brake forming uniform beads.

equations of the same form used in the general instability analysis.

Material Yield

Material yield is determined from combined axial compression, bending, and shear stresses at the panel center, using the effective stress intensity according to the Henky-von Mises yield criterion.[12] The effective stress intensity is also used in determining plasticity correction factors for buckling stresses which are greater than the proportional limit of the material.

OPTRAN Code

Various beaded and tubular panel cross-section configurations were optimized for the above design conditions and the weights of those designs were compared to select the most efficient concepts. The optimizations were accomplished using the general design computer code OPTRAN (OPTimization by RANdom search algorithm)[6] which establishes designs by random selection of values in the dimensional parameters from specified search ranges. Minimum gage design constraints are accomplished by proper specification of the search ranges. The OPTRAN code makes possible investigations of effects of various design restraints that would otherwise be quite difficult when large numbers of variables are involved. The number of variables is limited only by computer time.

Designs optimized for load conditions, 1) and 2) are critical in local instability over most of the combined load

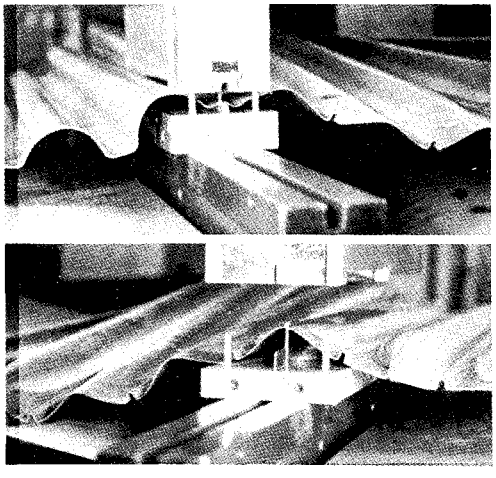

Fig. 4 Reforming panel end closures.

failure surface. If the panel length is increased general instability begins to dominate more of this failure surface, but the panel design is no longer optimum. When the panel design is reoptimized for the increased length it is found that the local instability modes again predominate. Also, when individual parameter changes are arbitrarily made to an optimized design, efficiency is decreased, but the individual parameters can be restrained and the design reoptimized with relatively little loss in efficiency. This is particularly significant because nominal gage material or standardized bead pitch can be used with minimum loss in efficiency.

IV. Fabrication Development

Conventional methods of fabricating panels with trapped beads have been by hydro-press or matched die processes where all bead elements for the full panel are formed in a single operation. Some associated disadvantages are: 1) separate full size dies are required for each panel, 2) elongation limits prevent forming deep beads, and 3) material thinning occurs at the crests of the beads where they are strength critical.

Studies made to determine methods of producing deep multiple large-arc beads resulted in progressive brake forming corrugations, as shown in Fig. 3, and then reforming the ends. The approach is practical for fabrication of test parts and for production. Note that the bends are formed by a wrapping action which minimizes thinning and forming forces but results in considerable spring back. The $2t$ bead-to-flat bend radius was increased to approximately $10t$ at the ends so that the end closure could be accomplished without memory of the previous mold line. The compound contours of typical end closures are formed with net-dimensional tooling (no springback) as shown in Fig. 4. One problem encountered with end closure forming is compressive wrinkling associated with the compound contour in thin gage materials. The secondary bead, being formed in the upper portion of Fig. 4, is beneficial in reducing this compressive wrinkling as well as minimizing load-induced buckling which can occur in the large flat areas. An additional forming stage is applied to end closures when α is greater than 90° as shown in Fig. 2. The end closure is preformed to approximate shape, and finally the full end closure is sized in a female steel die using a high-energy-rate electro-hydraulic process (capacitor discharge through a spark gap in a water chamber). Assembly of the two sheet panels is accomplished by bonding in a fixture which restrains the two beaded sheets and the necessary doublers.

V. Design Evolution and Test

Development of the panel designs has been an evolutionary process. Selection of uniform section designs has been accomplished by the computerized design optimization processes while the end closure development has been a fabrication, test and modification process. This has been a very satisfactory combining of developmental processes. With good coordination and shop support the fabrication and testing of the end closure concepts is rapid, economical and produces very reliable results. Only a small percent of panel weight can be saved by refining end closures. A precise analysis of end closures is considered beyond the scope of this program. The rationale employed was that end closures should be sufficiently strong to withstand panel design loads and that their strength be verified by experiment.

Local Buckling Tests

Data to support the local buckling strength analysis was obtained by testing uniform section specimens, similar to

Table 1 Matrix of optimized test specimens

Design conditions: 1) 600 lb/in. C, 1 psi B, & 200 lb/in. S
2) 2000 lb/in. C, 2 psi B, & 400 lb/in. S
Test load conditions: C, B, S, C+B, C+S, B+S and C+B+S unless indicated otherwise

Configuration	Design condition	Fabricate	Test	Loads
		Panels 40 × 40 in.		
1a-1-P	1	4	3	all
2-2-P	2	3	3	all
2a-1-P	1	4	2	all
2a-2-P	2	4	3	all
		Local buckling specimens		
1a-1-U	1	9	7	all
2a-1-U	1	10	8	all
2a-2-U	2	10	8	all
		End closure specimens		
1a-1-E	1	1	1	S
2a-1-E	1	3	2	C, S
2a-2-E	2	4	3	C, S, C+S

that shown in Fig. 5, of each of the four cross sections plus a number of initial screening specimens. The specimens were potted at each end to facilitate loading in a combined load test fixture. Chords were attached to stabilize the edges and to reduce the in-plane bending stresses. Specimens of each configuration were tested in a fixture which applies separately (or simultaneously) uniform out-of-plane bending, axial compression and in-plane shear loads. The unsupported sections of the tubular local buckling test specimens are typically about 18 in. wide and 10 in. long. The single sheet specimens were made 30 in. long since their local modes are relatively long wave length.

End Closure Tests

The end closure development consisted of testing end closure specimens of each of several initial screening designs in addition to each of the configurations shown in Figure 2. Figure 6 shows a configuration 2a-2 fluted tube end closure test specimen with attachments and edge members to permit the specimen to be tested in shear and axial compression. The end closures were reinforced by fingered doublers bonded between the two beaded sheets, at the ends of the panels, with the fingers pointed toward the centers of the panels. Rivets were used to reinforce the bond against the peeling stresses induced by the shear loads.

Panel Tests

Full size 40 × 40 in. panels of each of the designs were fabricated and tested under combined loads. The combined load test technique is an extension of a system developed to test shear beams in support of the Boeing SST development program.[13] Compression is applied to the panel by two vertical actuators, and shear is applied by a horizontal actuator to the side of the test panel. An air bag system, located behind the test panel, is used to produce bending. Extensive finite element analyses were conducted to support the design of the test beam and its chords, joints, buffer bays and loading plates, to minimize the undesirable influences of the boundary members upon the stress distributions within the test panel. The inplane moment of inertia of the joints and the chords of the test beam were minimized in order to minimize the Vierendeel truss effect. It was necessary to provide enough lateral and torsional stiffness in the chord and joint members to prevent local instability in the boundary members. A rigid truss system and pivoted links were used to restrict the motion of the test beam to a single plane and prevent general instability in the beam.

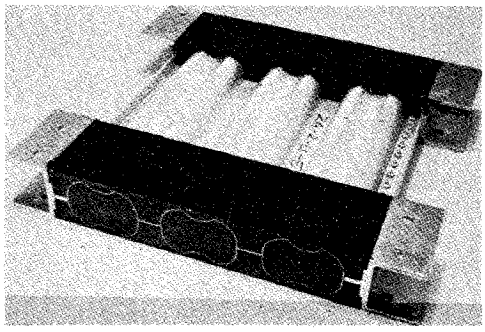

Fig. 5 Local buckling test specimen.

The matrix of end closure, local buckling and panel test specimens corresponding to the four final configurations is shown in Table 1. The table omits the various test specimens used for concept screening.

VI. Instrumentation

Varying amounts of instrumentation were used with the different test specimens to permit monitoring of stresses, out-of-plane deflections and the associated failure modes.

Approximately 70 strain gage channels were installed for the first panel test to establish that uniform strain distributions were realized in the test specimen. These precautions were considered necessary to assure uniform stress distributions within the test panels, to simplify the correlation of the test results and to prevent premature failure in the boundary. The failures have generally initiated at the center rather than the edges of the test specimen indicating that satisfactory boundaries were achieved. Approximately 30 strain gage channels were used to monitor stresses in subsequent panel tests.

End closure specimens were strain gaged only when investigating particular problems. Correspondingly, the number of strain gages used with the local buckling test specimens ranged from none for the initial screening test specimens loaded only in shear to approximately 24 for the final combined load test specimens.

Although the strain gage data constituted a necessary part of the test data, the grid shadow Moiré monitoring technique[14] was far more helpful in identifying detailed failure modes. The Moiré monitoring technique was used in the initial end closure development effort to identify the occurrence and nature of deformations associated with the different end closure designs. Moiré was also used in conjunction with the local buckling tests and the full size panel tests to identify the various buckle modes as they developed.

VII. Test Technique

Force/Stiffness Application

Both the quantity and quality of the test data available from this program were enhanced by the Force/Stiffness

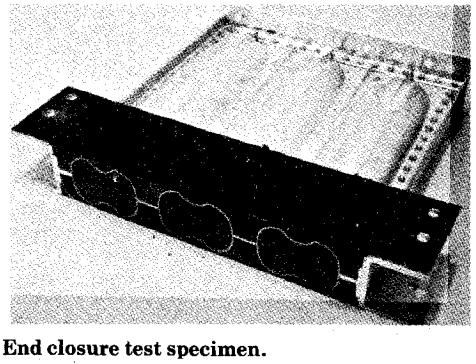

Fig. 6 End closure test specimen.

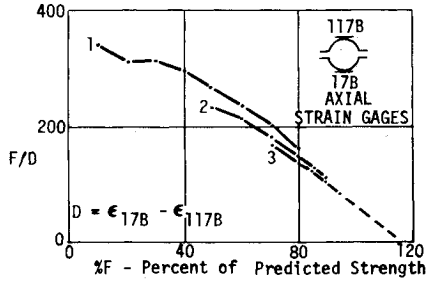

Fig. 7 Force/stiffness plot.

(F/S) nondestructive buckling test technique.[7] The F/S technique permits monitoring during the test to observe proximity to and magnitude of the critical buckling load without failing the test specimen.

Figure 7 shows an F/S plot developed for test panel 2-2-P-1 when it was being loaded in pure axial compression during three separate tests. The "stiffness" parameter, obtained by dividing the applied load by observed deflections, is plotted versus the applied load or "force." The deflection parameter used in Fig. 7 is the difference in output from two strain gages located on the front and rear crests of the bead in the center of the panel. This local bending strain is proportional to the out-of-plane deflection, and tends to increase without limit as the critical buckling load is approached. The F/S plot extrapolates to the horizontal axis at the critical load. Details of the application of the F/S method, particularly its application to local buckling predictions, are given in Ref. 7.

Test Procedure

The F/S technique permitted identification of failure loads for many load conditions for individual test panels. This permits the matrix of load conditions shown in Table 2 to be applied and the corresponding strength level for each of those conditions to be verified for each test panel. In order to obtain the best possible accuracy, the load conditions are applied in sequence to a given percentage of the predicted strength. F/S predictions are made from these data. The percentage is then increased and the load conditions are repeated. Improved F/S predictions are made from the additional (higher load) data as indicated by curves 2 and 3 in Fig. 7. Finally, the specimen is tested to failure in a selected load condition. The failure test provides a check on the F/S predictions. The ability to define numerous failure loads on a single specimen removes inaccuracies which result from specimen-to-specimen differences. Consequently, major improvements in quality of the test data and in ability to correlate test results with the analytical predictions are realized.

VIII. Test Results

While large amounts of test data have been generated to date on all of the optimized configurations, as well as earlier screening configurations, most of the data are from end closure and local buckling specimens. Tests on the large 40 × 40 in. panels are completed on the circular tubular configuration only. Therefore while specified failure peculiarities will be discussed in this section for all configurations, buckling test data on large panels and correlation with theory will be restricted to the circular tubular panels only.

Table 2 Panel test load conditions

Test load condition	Load ratio N_x	Load ratio N_{xy}	Pressure (const.) P (psi)
1	1	0	0
2	0	1	0
3	1	1/5	0
4	1	1/3	0
5	1	0	1.00
6	1	0	2.00
7	0	1	1.00
8	0	1	2.00
9	1	1/5	1.00
10	1	1/5	2.00

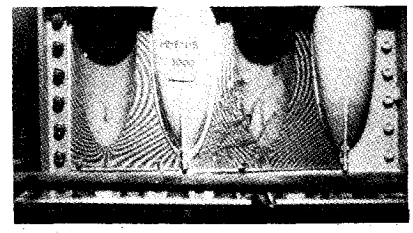

Fig. 8 Shear test of single sheet end closure specimen.

Failed Test Specimens

A number of photographs of loaded or failed test specimens are shown. Figure 8 shows a single sheet end closure test specimen loaded in shear and monitored using grid shadow Moiré. The specimen performed quite well under axial load. However, the Moiré patterns indicate that shear loading produced large out-of-plane deflections. The deflections are due to a discontinuity in the local shear center which results in out-of-plane couples without adequate reaction. Addition of stiffening elements such as fish plates and transverse and longitudinal beams reduced the deformation, but not satisfactorily. Further tests and analyses are required to resolve this problem. Figure 9 shows a configuration 2a-1 end closure specimen which failed in axial compression. Note that failure occurred as local crippling in the uniform section rather than in the region of the end closure thereby demonstrating adequate end closure strength. Figure 10 shows a large panel failed in combined axial compression and shear.

Figure 11 shows the upper edge of panel 2-2-P-3 which buckled in the end closure adjacent to the joint splice due to lateral pressure and axial load. Large panel behavior is further discussed under "Circular Tube Configuration Results" below.

Failure modes of particular interest are the buckling modes observed during compression tests of the single sheet panel specimens. These modes, shown graphically in Fig. 12, have axial half-wave lengths generally small with respect to typical panel lengths. Panel failure occurring as a result of this mode of buckling is seen in the longer specimen in Fig. 13. This type of buckling behavior was also reported in Ref. 15. In Fig. 12a and 12b the modal behavior is seen to be similar to buckling of a simply supported orthotropic strip whose midplane axis coincides with a diagonal drawn between alternate bead crests, and is therefore called the "diagonal" buckling mode. The mode shape of Fig. 12c, which is also considered a "diagonal" mode, is observed in tests of the fluted bead specimens. The mode shown in Figs. 12a and 12b is antisym-

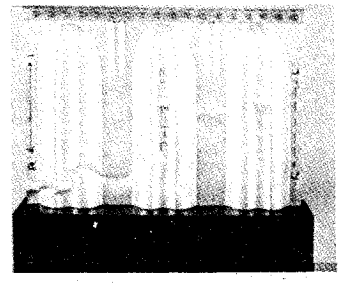

Fig. 9 End closure compression failure.

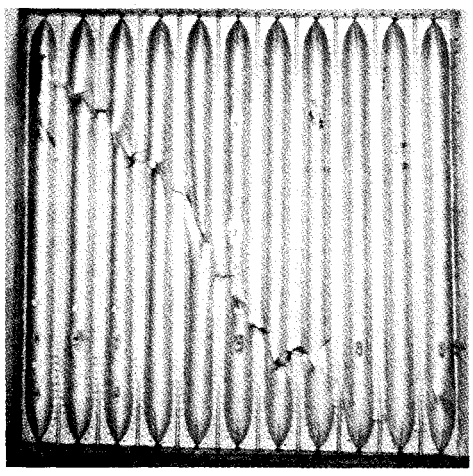

Fig. 10 Panel combined load failure.

metric with respect to axes of the bead cross section as opposed to the mode in Fig. 12c which is symmetric. The axial wavelength is shorter for the mode of Fig. 12c than for those of Figs. 12a and 12b, the former exhibiting four half waves in a typical 30-in. test panel length, while the latter generally show two.

The diagonal mode exhibits some characteristics of a panel general instability mode. The entire panel is usually involved and significant growth of the modal deflection pattern occurs prior to panel buckling. This behavior is often accompanied by an apparent change of mode at an intermediate load level from $n = 1$ to $n = 2$.

The diagonal buckling mode has been observed in panels loaded in pure shear, although the exact character of the mode is difficult to determine. One characteristic common to all configurations tested in shear is that no significant growth of buckled mode appears to occur prior to panel failure, and the actual failure exhibits skewed, short wave length shear buckles, typical of conventional local buckling or crippling failures. An example of a circular tubular local buckling specimen failed in shear is shown in Fig. 14.

In the two sheet configurations no mode of the diagonal type was expected and none was observed in the panel tests. However, in the fluted tube specimens a different mode of interest has been observed. Test of a full size, 40 × 40 in. panel of the configuration 2a-1 fluted tube exhibited a pronounced tube flattening mode.

Force/Stiffness data indicated premature failure of the panel in general instability at approximately 70% of the predicted failure load. This reduction is attributed to loss of sectional properties resulting from the tube flattening mode. After this behavior was identified, internal post stiffening was added on six inch centers to prevent flattening. Subsequently, when the panel was tested to failure, it developed 100% of the design loads. Thus it appears that an efficient modification to prevent tube flattening may be necessary if the fluted tube concepts are to attain their potential efficiency. Study of the fluted concepts is not yet complete.

Fig. 11 Panel edge combined compression and pressure failure.

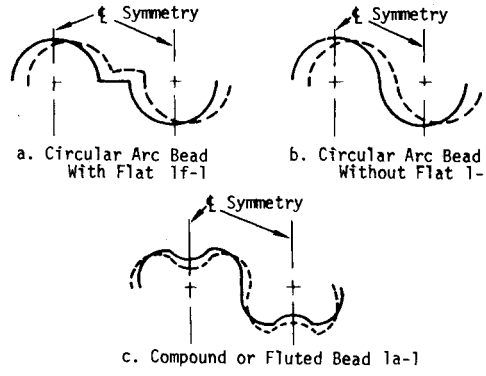

Fig. 12 Single sheet buckling modes.

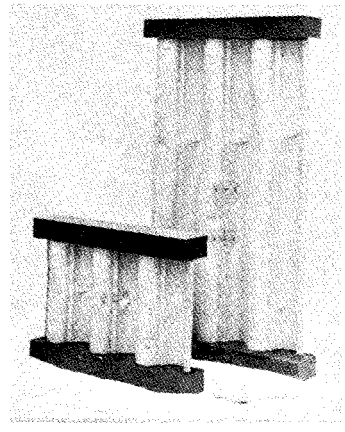

Fig. 13 Local buckling compression failures.

Circular Tube Configuration Results

The circular tube configuration is the only configuration for which the scheduled testing has been completed. This testing has included two end closure tests, five local buckling tests and tests of three 40 × 40 in. full size structural panels. A summary of these test results compared with analytically predicted strengths is presented in Table 3. Extensive nondestructive testing of the full size panels was accomplished in different loading conditions; however, only the results of the final tests to failure are presented here. The end closure and local buckling specimen geometries are from early screening studies, while the geometry of the full size panels is from a final optimum design scaled down to the nearest standard material gage. The detailed geometries are shown in Table 3. In the analytical strength predictions original analysis refers to the theory used in obtaining the final OPTRAN panel designs and weight/strength curves, while the experimental modification refers to the revised analysis which is described in Section IX, Modified Failure Criteria. The correlation of test results with the modified analysis is excellent. Only one test point shows the analysis to be unconservative, and that by only 3%.

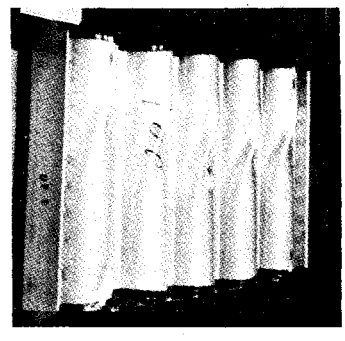

Fig. 14 Local buckling shear failure.

Table 3 Circular tubular results and analytical predicted strengths

Specimen no. ▷	Failure test condition	Ultimate stresses — ksi: Test	Analysis: Original	Analysis: Exp. mod.
2-2-E-6	Shear	$F_S = 25.0$	—	—
2-2-E-8	Compression	$F_C = 49.1$	—	—
2-2-U-1	Bending	$F_B = 78.2$	$F_B = 77.6$	$F_B = 77.6$
2-2-U-2	Shear	$F_S = 37.5$	$F_S = 35.0$	$F_S = 35.0$
2-2-U-3	Compression	$F_C = 69.2$	$F_C = 75.4$	$F_C = 67.8$
2-2-U-4	Compression	$F_C = 58.5$	$F_C = 63.1$	$F_C = 60.3$
	+ Shear	$F_S = 17.8$	$F_S = 19.2$	$F_S = 18.4$
2-2-U-5	Compression	$F_C = 21.8$	$F_C = 20.4$	$F_C = 19.8$
	+ Bending	$F_B = 58.8$	$F_B = 55.0$	$F_B = 53.4$
2-2-P-1	Compression	$F_C = 37.8$	$F_C = 30.7$	$F_C = 36.0$
	+ Shear	$F_S = 12.9$	$F_S = 10.5$	$F_S = 12.3$
2-2-P-2	Compression	$F_C = 37.5$	Panel edge failure	
2-2-P-3	Shear	$F_S = 17.6$	$F_S = 13.6$	$F_S = 17.6$

[a] ▷ Specimen number identification
X-x-x-x Bead design type, see Fig. 2
x-X-x-x Design load condition
x-x-X-x Specimen type, see Table 1
x-x-x-X Type or sequence of test

Nominal bead configurations
2-2-*E-x*:
2-2-*U-x*: $R = 1.20$ in., $t = 0.032$ in., $\alpha = 85°$
2-2-*P-x*: $R = 1.34$ in., $t = 0.025$ in., $\alpha = 90°$

Panel 2-2-P-1 was tested at each of the ten loading conditions in Table 2 and then was loaded to failure at a combined compression and shear load that reached approximately 128% of the predicted strength. The failed panel is shown in Fig. 10. The failure extended across the panel center but did not extend through the edges. Panel 2-2-P-2 had been tested at each of the ten load conditions and was loaded to 94% of the predicted strength in axial compression, which was considerably above the axial load component for the design load, when the panel failed in the end closure adjacent to the joint. Panel 2-2-P-3 had been tested at each load condition and was loaded to 98% of the predicted strength in axial compression plus pressure when it failed in a manner similar to that of panel 2-2-P-2. The failed edge, shown in Fig. 11, involved buckling but no tearing of the metal. The panel was again loaded in pure shear and the F/S plot was virtually unchanged, indicating that the shear strength was unaltered. The shear load was increased until failure similar to that shown in Fig. 10 occurred in the lower half of the panel at 130% of the analytically predicted panel strength.

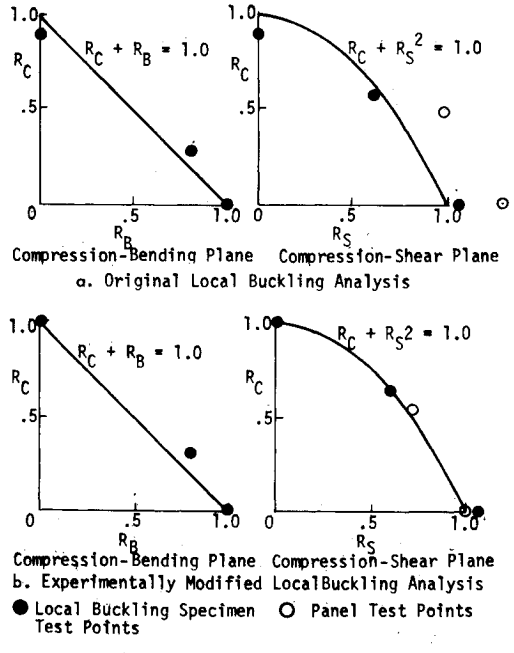

Fig. 15 Local buckling interaction curves for circular tubular panel with test points.

IX. Modified Failure Criteria

Figure 15 shows the correlation of test data with analysis both before and after experimental modification. The modifications to the analysis affect the bead crippling stress equations in compression and shear. A knockdown factor of 0.9 is applied to the buckling coefficient in the equation for bead compression crippling, Ref. 10. The buckling coefficient in the equation for bead shear crippling is also modified as follows:

$$K_s = 3.3Z^{0.585} \qquad (Z > 10)$$

This modification is primarily a change in the length effect which is represented by a series of curves for K_s as a function of Z and a/b (see Ref. 11). The improvement in correlation between test and analysis can be seen graphically by comparing Fig. 15a with Fig. 15b. The R values shown in these figures were taken directly from the test and analysis results which are summarized in Table 3.

Figure 16 shows the weight/strength curve for the circular tube panel from Fig. 1 with the corresponding curves for fluted panels. The dashed-line curve in Fig. 16 shows the effect of the modified failure criteria on the optimum weight of the circular tube panel. Although the allowable local buckling strength in compression was reduced, the increased shear strength results in a weight reduction of approximately 3% for the specified design load condition. Tests and data analysis remain to be completed before the

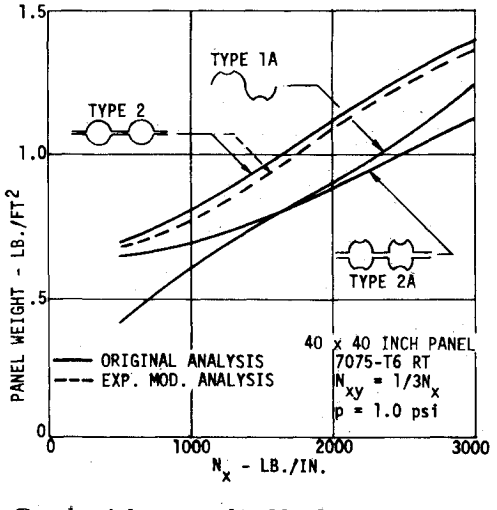

Fig. 16 Panel weight vs panel end load.

potential of the more efficient fluted designs can be established.

X. Conclusions

A contractual study was initiated to exploit the efficiency of curved elements in the design of panels to cope with the thermal environment. The goal to develop design theory and modify this theory with test data on optimized configurations has been essentially attained for a circular tube configuration. Test data obtained under combined loading on local buckling specimens and on large panels show excellent agreement with theory. The beaded and tubular panel concepts, selected primarily because of their tendency to minimize thermal stresses, are far more efficient than conventional stiffened sheet construction and appear to be competitive when compared with fabrication costs of other panel concepts. The fluted designs, which are still under investigation have the potential to be even more efficient than the circular designs. Successes with the specific concepts developed during this program suggest that much broader applications of the beaded and tubular panel concepts warrant additional considerations.

Boeing has initiated an IR&D program to develop welded circular tube end closures from thin 6A1-4V titanium sheet and to investigate the use of panels with one beaded sheet and one flat sheet in order to further extend the areas which utilize the technologies obtained from this program. Although the work that is being accomplished was initiated to support advanced space vehicle concepts, it is apparent that these developments in beaded and tubular panels should result in increased efficiency in many types of future vehicles. Once again research initially directed toward the space effort will undoubtedly result in even greater non-space benefits.

References

[1]Shideler, J. L. and Jackson, L. R., "Fuselage and Tank Structures for Hypersonic Aircraft," *Conference on Hypersonic Aircraft Technology*, Ames Research Center, Moffett Field, Calif. SP-148, May 1967, NASA.

[2]Anderson, M. S., Robinson, J. C., and Klich, G. F., "Analysis of Wing Structures for Hypersonic Aircraft," *Conference on Hypersonic Aircraft Technology*, Ames Research Center, Moffett Field, Calif. SP-148, May 1967, NASA.

[3]Plank, P. P., Sakata, I. F., Davis, G. W., and Richie, C. C., "Hypersonic Cruise Vehicle Wing Structure Evaluation," CR-1568, May 1970, NASA.

[4]Card, M. F., Davis, J. G., and Shideler, J. L., "Advanced Design Concepts for Shuttle Airframe Structures," NASA Space Shuttle Technology Conference, San Antonio, Texas, April 12-14, 1972, NASA TM X-2570, July 1972.

[5]Shideler, J. L., Anderson, M. S., and Jackson, L. R., "Optimum Mass-Strength Analysis for Orthotropic Ring-Stiffened Cylinders Under Axial Compression," TN D-6772, July 1972, NASA.

[6]Laakso, J. R., "Design Synthesis of a Boron/Epoxy Reinforced Metal Shear Web," AIAA/ASME/SAE 13th SDM Conference, San Antonio, Texas, April 10-12, 1972.

[7]Jones, R. E., Greene, B. E., "The Force/Stiffness Technique for Nondestructive Buckling Testing," AIAA/ASME/SAE 15th SDM Conference, Las Vegas, Nev., 1974.

[8]Musgrove, M. D., Mortensen, R. E., "Development of Titanium Structural Element Allowables For The Boeing SST," AIAA/ASME 11th SDM Conference, April 1970, Denver, Colo.

[9]Timoshenko S. P., Gere, J. M., *Theory of Elastic Stability*, 2nd ed., McGraw-Hill Book Co., New York, 1961.

[10]"Buckling of Thin-Walled Circular Cylinders," SP-8007, 1965, revised 1968, NASA.

[11]Gerard, G. and Becker, H., "Handbook of Structural Stability, Part III-Buckling of Curved Plates and Shells," TN-3783, 1957, NASA.

[12]Nadai, A., "Theory of Flow and Fracture of Solids," Vol. I, 2nd ed., McGraw-Hill Book Co., New York, 1950.

[13]Mello, R. M., Sherrer, R. E., Musgrove, M. D., "Intermediate Diagonal Tension Field Shear Beam Development For The Boeing SST," AIAA/ASME 12th SDM Conference, April 1971, Anaheim, Calif.

[14]Dykes, B. C., "Analysis of Displacements In Large Plates By The Grid-Shadow Moiré Technique," *Fourth International Conference on Stress Analysis*, April 1970, Cambridge, England.

[15]Plank, P. P., Sakata, I. F., Davis, G. W., and Richie, C. C., "Substantiation Data For Hypersonic Cruise Vehicle Wing Structure Evaluation," CR-66897-2, -3, Feb. 1970, NASA.

FEBRUARY 1974 J. AIRCRAFT VOL. 11, NO. 2

An Automated Procedure for Computing Flutter Eigenvalues

Robert N. Desmarais* and Robert M. Bennett*
NASA Langley Research Center, Hampton, Va.

A new, fast, and economical automated procedure for implementing the traditional *V-g* method of flutter solution is described. The procedure requires as input the generalized aerodynamic forces for a range of reduced frequencies obtained from an aerodynamic program. These aerodynamic forces are interpolated with respect to reduced frequency using a newly developed, partially tabulated cubic spline that is both fast in execution and economical in storage. The flutter solution is then obtained using an eigenvalue routine that has been developed to take advantage of the parametric nature of the V-g type of solution. Furthermore, the routine takes care of the fundamental and troublesome problem of properly sorting the output eigenvalues. By solving the root-sorting problem, the interpolation for flutter crossings and automatic plotting are accomplished efficiently. The computational techniques used in this new program are described and some sample results are given.

Presented as Paper 73-393 at the AIAA/ASME/SAE 14th Structures, Structural Dynamics, and Materials Conference, Williamsburg, Va., March 20-22, 1973; submitted July 2, 1973; revision received December 12, 1973.

Index categories: Aircraft Vibration; Nonsteady Aerodynamics; Aeroelasticity and Hydroelasticity.

* Aerospace Engineer, Structures and Dynamics Division. Member AIAA.

Nomenclature

A_i = tabulated spline coefficients

A_{ij} = generalized aerodynamic force matrix element resulting from the pressure induced by the jth mode acting through the displacements of the ith mode

B_i = $Y_i - Y_i''/6$ where $Y(X)$ is the function being interpolated